Composites Science and Technology 215 (2021) 109030

Contents lists available at ScienceDirect

Composites Science and Technology

journal homepage: www.elsevier.com/locate/compscitech

Characterising microstructural organisation in unidirectional composites

S. Gomarasca [a,*], D.M.J. Peeters [a], B. Atli-Veltin [a,b], C. Dransfeld [a,*]

[a] Department of Aerospace Structures & Materials, Delft University of Technology, Kluyverweg 1, 2629, Delft, Netherlands
[b] TNO, Stieltjesweg 1, 2628 CK, Delft, Netherlands

ARTICLE INFO

Keywords:
A. Carbon fibres
A. Polymer-matrix composites (PMCs)
D. X-ray computed tomography
Microstructure

ABSTRACT

Understanding the three-dimensional variability of unidirectional composites is relevant to the material performance and the development of advanced material modelling strategies. This work proposes a new methodology for the characterization of unidirectional composites, showcased on carbon fibre/poly(ether-ether-ketone) tapes. Three microstructural descriptors were here introduced, each representing an increasing level of complexity in the fibre architecture: from a tortuosity-based single fibre trajectory analysis to fibre groups' behaviour, to fibre network interconnectivity. The methodology was developed and validated on real material datasets acquired via X-ray computed tomography. A facile method for image analysis was used to reconstruct the three-dimensional fibrous architecture at a single fibre path resolution. The approach bridges a gap in the traditional approach and nomenclature typical of the composite field to describe and quantify complex fibre organization in unidirectional composites, highlighting micro- and mesoscopic features, such as edge-core effects in the fibre arrangement, possibly occurring in tow spreading. The study of the parameter interdependence showed relationships, which will provide further insight for future research in the study of microstructure formation of unidirectional composites, its evolution during processing or loading, and input for advanced modelling techniques based on Representative Volume Elements.

1. Introduction

Microstructural features are relevant for understanding and modelling unidirectional composites (UDCs) performance [1]. Size effects [2], microscale variability [1,3–6], and local fibre orientation [7–12] do have an impact on mechanical properties [13,14] and processability [15]. In particular, understanding the three-dimensional (3D) variability in the fibre arrangement of UDCs was highlighted for its importance in advanced material modelling [14,16]. Different routes are available for the reconstruction of the 3D unidirectional microstructure. Optical microscopy slicing works with the acquisition of several images along the length of the UDC by performing cyclic grinding and polishing steps [17]. This method is however labour-intensive and leads to destructive alteration of the specimen. X-ray based techniques such as X-ray Computed Tomography (XCT) and Synchrotron Radiation Micro-Computed Tomography (SRCT) have been receiving increasing interest for their ability to capture volumetric data with high automation. Even though characterized by a lower contrast between fibre and matrix and by reconstruction artefacts, successful post-processing of the obtained volume was performed via individual fibre tracking [18–20], Digital Image Correlation [14,20], and homogenisation tensor [21,22]. Single fibre paths tracking comes with challenges related to the high resolution and contrast required to identify single fibre centres, especially in carbon fibre composites, where the fibre diameter is typically in the order of 7 μm [23]. It has however the advantage of a full 3D reconstruction of the fibre architectural arrangement, and the possibility to correctly attribute properties to single fibres.

Recent work highlights the relevance of understanding micro- and mesoscopic features in the fibre organisation, hinting at the emergence of complex fibre movements. Fritz et al. [24] used XCT to analyse the microstructure of intralaminar tow-aligned resin rich pockets, which are intra-tow features that were theorised to be related to spreading, and on the characterization of intralaminar sub-microvoids in aerospace grade composites. 'Stray fibres' have been observed at the ply interface, typically showing greater deviation from the main unidirectional orientation by crossing the path of multiple fibres [24]. Zehnder et al. performed reconstruction of single fibres based on XCT data in bent unidirectional samples via particle tracking algorithms. The work highlighted challenges in tracking fibres in media with small features and low contrast between the different constituents, which is made

* Corresponding authors.
E-mail addresses: S.Gomarasca@tudelft.nl (S. Gomarasca), C.A.Dransfeld@tudelft.nl (C. Dransfeld).

https://doi.org/10.1016/j.compscitech.2021.109030
Received 26 July 2021; Received in revised form 25 August 2021; Accepted 26 August 2021
Available online 6 September 2021

worse by bending [23]. Mehdikhani et al. analysed SRCT data via both DIC and single fibre tracking to map local fibre misalignment, quantifying differences in the in-plane and out-of-plane direction [14]. In the work of Emerson et al., SRCT was used to evaluate the in-situ behaviour under compression loading using a single fibre tracking algorithm [18], observing the evolution of micro-buckling and kinking at different load steps [19]. They were able to qualitatively show spatial variations in the azimuthal fibre alignment with increasing load, showing a tendency to an increase in both fibre misalignment with the axial direction and global twisting of the fibre network. Wang et al. expanded this study by using XCT analysis to further studying segregation effects in the fibre alignment and local buckling by means of k-means clustering [25]. The work of Fast et al. represents one of the most comprehensive efforts to quantify microstructural variability in fibre reinforced composites following single fibre tracking [26]. The authors employed topological and euclidean metrics to characterize unidirectional composite volumes acquired via SRCT. The analysis addressed the quantification of both traditional descriptors such as local fibre volume and orientation, as well as less explored concepts such as Voronoi fibre neighbourhood analysis, to highlight clustering in fibre neighbours association.

Even though complex fibre arrangements are observed, the parameters used to quantify these phenomena are mostly still bounded to a traditional approach and nomenclature typical of the composite field. By looking into other research domains, new approaches for investigating these features can be found.

In the context of studying the permeability of fibre bundles, tortuosity was defined as the ratio between the distance covered by the fluid during permeation and the distance as if it was a straight line [27]. Tortuosity was also used by Wojciech et al. to characterize gas transport kinetics regimes through randomly oriented carbon nanotube arrays [28]. This is a local parameter that can provide insight on differences in functional organisation. In the study of the collagen fibre architecture of the eye, the same definition was applied to map local variations for the identification of different functional regions [29]. The concept of tortuosity has however not been applied yet to study fibre organisation in unidirectional composites, but could prove useful in mapping local variations in their arrangement. This might both help characterizing the mechanisms of microstructure formation, and the micromechanical effect of local variability in fibre alignment.

The understanding of patterns in collective fibre organisation has not been well addressed in fibre composites literature. This would however be relevant to gain a greater understanding of the microstructure formation, spatial organisation and evolution. In biological sciences, the study of collective organisation is conducted in relation to animal locomotion [21,30]. Various descriptors are used to characterize collective phenomena, from vorticity in bacteria assembly [31] to coherent directional motion parameters [32], to velocity correlation functions for hierarchies in birds flocking motion [33]. Similar models could help to capture local order regions in materials of engineering interest. For unidirectional composites, such descriptors could be used to study both microstructural formation and local variability in the fibre arrangement in the length direction of the UDC, using in this case an analogy between time and axial position.

The study of the architectural interconnectivity of fibrous materials can further add to understanding its morphology. In silkworm cocoons, for example, greater fibre orientation with the tensile direction and higher fibre intersection densities appear to contribute to higher tensile performance [34]. Edge-core effects in the local fibre content are also observed, with a decreasing fibre volume from the centre to the edges. The fibre intersection density was also evaluated in the architecture of bird nests to characterize their network [35,36], by tracking the number of contacts between straws. A similar approach was used by Viguie et al. to study fibre contacts in fibrous material of diverse origins, from glass fibres to cellulosic fibres [37]. Fast et al. applied a similar concept to study of unidirectional microstructures, hypothesising an effect on the fracture toughness of composites [26].

This work takes a step forward in the 3D characterization of UDCs to elucidate their microstructural complexity. The aim is to develop new approaches for more advanced quantification of complex phenomena such as microstructure formation and evolution, and for the generation of RVE for advanced material modelling. This is done by introducing novel descriptors which address the local fibre architecture at an increased level of complexity. Such descriptors are based respectively on the concepts of tortuosity, collectivity in the fibre motion, and length of neighbourhood to quantify the network interconnectivity. Section 2 addresses the reconstruction of the 3D fibre architecture of unidirectional fibre composites. X-ray computed tomography was used for the image acquisition, and a facile method for image analysis was used for the 3D data reconstruction. Section 3 introduces the novel parameters used for the fibre path analysis. The results of the application of the methodology to selected UDCs, and the discussion of the identified hierarchies and parameter interdependence, can be found respectively in Section 4 and 5. Conclusions and indications for future work will be addressed in Section 6.

2. Methodology

The methodology developed is based on computational image analysis of real material datasets. The purpose of this section is to identify an analysis workflow that can be applied to similar unidirectional materials, such as continuous fibre-matrix systems.

2.1. Sample preparation

The methodology was showcased by using two commercial aerospace-grade unidirectional tapes of carbon fibre and poly(ether-ether-ketone). The tapes have a nominal fibre volume fraction of 59% and 47% respectively, and a thickness of 150 μm and 200 μm, and hereby called Tape A and Tape B. Samples of 10 mm in fibre direction and 1.5 mm in width direction were harvested from a larger tape roll.

2.2. Tomographic image collection

The data reported was acquired via X-ray micro-computed tomography with a Zeiss Xradia 520 Versa, which is a state of the art instrument used in recent literature [10,18,23–25,38]. A resolution of 0.7232 μm, corresponding to about 10 pixels per fibre diameter, was selected to facilitate single fibre identification similarly as in previous work [18,19,23,24]. A 2000 $\times$ 2000 pixel detector in binning mode 2 was used with a 4$\times$ magnification lens, leading to a resulting scan volume of approximately 700 μm by 200 μm in the tape cross-section and 723 μm in the tape length direction. A voltage-to-power ratio of 100/9 kV/W and an exposure time of 6 s were used for the image acquisition. A representative cross-section of the two materials is shown in Fig. 1a) and b). The measurement was repeated three times in the fibre length direction, and the volumes were stitched together to cover a total tape length of about 1800 μm, of which about 1450 μm have been used for the following analysis. The datasets are available at DOI: 10.4121/16437297.

2.3. Fibre path reconstruction

The reconstructed volume was processed by Fiji software plugins [39]. Linear stack alignment with Scale Invariant Feature Transform (SIFT) [40] was used for image registration to correct for sample tilt. The workflow for fibre path reconstruction after this step is showcased for the case of Tape A in Fig. 2. To correctly distinguish fibres from local reconstruction artefacts, fibre segmentation was performed via Trainable Weka Segmentation [41], a machine-learning-based tool that allows for image classification based on a training set provided by the user. Approaches based on automated feature recognition based on training sets was also used in recent literature [18,19,25]. A training set of three slices was employed with classification in two classes – fibres

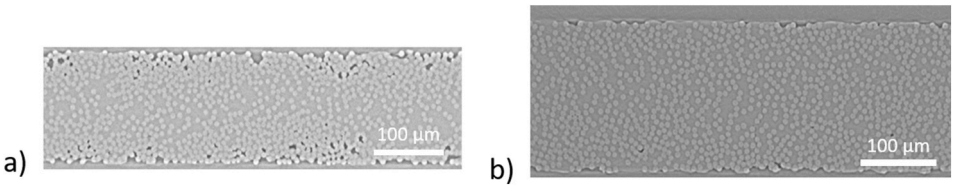

Fig. 1. X-ray computed tomography cross-section of a) Tape A and b) Tape B.

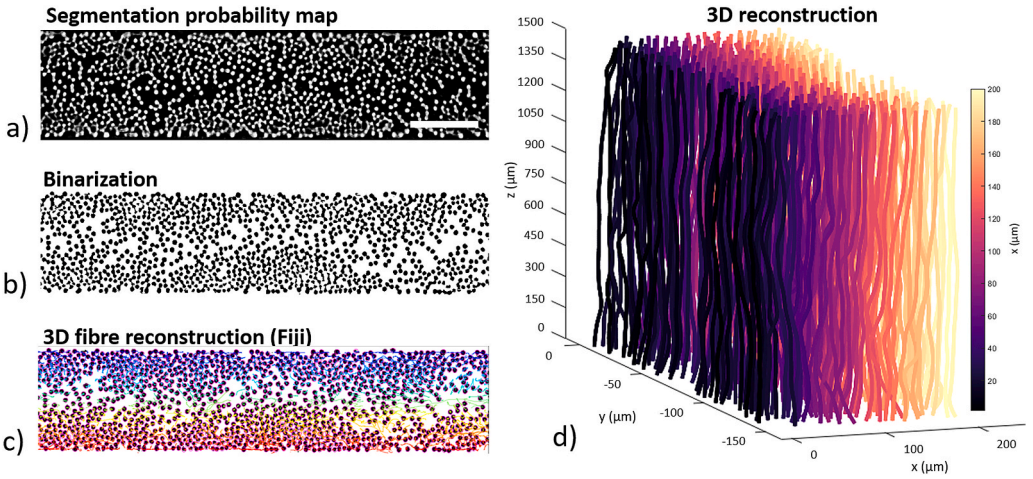

Fig. 2. Workflow for image analysis and fibre path reconstruction, based on Tape A a) Image segmentation, conducted with Trainable Weka segmentation. The scalebar in white indicates a distance of 100 μm b) Image binarization via thresholding c) fibre path reconstruction using Trackmate, colour-coded according to the average through-thickness position of the fibre paths d) 3D reconstructed fibres for a portion of the tape, colour-coded along the tape width direction. (For interpretation of the references to colour in this figure legend, the reader is referred to the Web version of this article.)

and not-fibres - which was then applied to the full dataset. The output of the segmentation is a probability map, which can then be further processed. An example is shown in Fig. 2a), where the locations with a higher chance to be associated with fibres are highlighted with a lighter colour in the greyscale image. A data reduction scheme was then applied by averaging groups of 10 consecutive probability maps (equivalent to 7.2 μm in the fibre direction) to lower the computational cost of the following steps and to increase accuracy by further mitigating the effect of segmentation artefacts and noise.

Image thresholding was then performed, leading to a binarized result as in Fig. 2b), followed by fibre path reconstruction via the plugin TrackMate [42]. TrackMate is a tool originally designed for cell biology to track single entities in time-resolved problems. This approach can be adjusted to track fibre centre translation between slices. Since the measurement is 'space resolved' rather than 'time resolved', the result will be later interpreted by exchanging the time coordinate with the relative axial coordinate along the tape length. The tool employs a two-steps approach for fibre track reconstruction: fibre centre identification, followed by fibre centre linking. For the first step, a Difference of Gaussian filter was used. For the second step, a Linear Motion LAP (Linear Assignment Problem) tracker was used. This method is based on the use of a Kalman filter for the identification of the most probable position of the fibre in consecutive cross-sections. Analogous approaches have been already used for similar problems in the composite field [17,20] and are quite established in the life sciences environment for particle tracking [21,43].

A search radius of 10 μm and maximum gap linking distance of 16 steps (corresponding to about 115 μm) were used. Consistently with the data reduction scheme used, the fibre centres determined are spaced of 7.2 μm in the tape longitudinal direction.

A map showing the resulting analysed tracks, colour-coded according to their average thickness position, is showed in Fig. 2c). The coordinates of fibres which could be followed entirely through a region of 1450 μm were extracted and imported in MATLAB for further analysis. This led to detection of about 80% of the theoretical number of fibres for the given material volume. This does not consider fringe fibres at the side edges of the tape, which might not be fully imaged, and therefore were not fully reconstructed [26]. A portion of the resulting fibre distribution is shown for Tape A in Fig. 2d).

3. Microstructural descriptors

Three parameters are introduced for the analysis of the microstructural variability of UDCs: differential tortuosity, collective motion, and length of neighbourhood. They represent respectively information on single fibre trajectory, similarities in fibre paths to identify group motion, and network interconnectivity within the material, addressing the architectural study of the material starting at a single fibre level towards an increasingly larger domain in the 3D space. The goal is to assess these parameters on the reconstructed fibre paths, understand their variability and explore interdependencies between them.

3.1. Differential tortuosity

In the context of studying the permeability of fibre bundles, tortuosity was used to quantify the deviation of the permeation trajectory from a straight path [27]:

$$\tau = \frac{L}{L_0} \tag{1}$$

where L is the distance covered by the fluid during permeation, and L_o the distance as if it was a straight line. By definition, this parameter is greater than 1, which corresponds to a perfectly straight fibre. For a unidirectional microstructure such as the ones object of study, the value of tortuosity is assumed to be close to unity [27]. The downside of this definition is that it does not allow to highlight the order of magnitude of the variation in local property.

An alternative definition is introduced in this work as differential tortuosity τ^d as a modification of Equation (1). Differential tortuosity represents the difference between the tortuosity of a real fibre and the tortuosity of an ideal straight fibre aligned longitudinally with the scan volume, and starts from a value of 0. This allows for a more intuitive

representation of highly aligned fibre populations via its order of magnitude, expressed in a logarithmic scale. Differential tortuosity is defined as:

$$\tau^d = \tau - 1 = \frac{L - L_0}{L_0} \tag{2}$$

where in this case, L represents the total length of the fibre and L_0 is the size of the scan volume.

A schematic is shown in Fig. 3. The total fibre length was measured as polygonal conducted through the fibre centre coordinates. For the data reduction scheme used, such points occur at an interval of $\Delta z = 7.2$ μm in the fibre length direction.

3.2. Collective motion

In the case of UDCs, collective motion equations could be used with the objective to study how the fibre architecture develops along their axial direction. Local synchronous motion patterns were characterized in biology through the collective motion parameter [32]:

$$\Phi(i,t) = \frac{1}{N_r}\sum_{j\in C_r}\frac{v_i(t)\cdot v_j(t)}{|v_i(t)|\ |v_j(t)|} \tag{3}$$

where C_r is the circle of radius r surrounding element i at time t, N_r is the number of elements j contained in C_r, and $v_i(t)$ and $v_j(t)$ are local velocities, whose directions are tangent to the trajectory of the respective element. By the definition of the dot-product, Equation (3) averages the cosine of the relative velocity vector angle between fibres $\cos\theta$ and is therefore sensitive to relative motion directionality. If orientation rather than the polarity of motion is relevant, $\cos\theta^2$ can be used to evaluate local order in studies of liquid crystal polymers alignment [32,44].

A variation from the literature parameter is introduced in this work for the analysis of UDCs in their axial direction to conduct the analysis in space along the fibre length rather than in time. The analysis is therefore not time-resolved but space-resolved. Moreover, the fibre neighbourhood is defined here according to a Voronoi tessellation [34,37]. The immediate neighbours according to the tessellation are considered for the averaging, consisting of the neighbouring cells which share an edge with fibre i.

This parameter is calculated for each fibre based on its surroundings for each 2D slice of the processed volume. The collective motion parameter CM for fibre i at the location z along the tape axis is defined as:

$$CM(i,z,\Delta z) = \frac{1}{N_{V_i}}\sum_{j\in V_i}\frac{d_i(z,\Delta z)\cdot d_j(z,\Delta z)}{|d_i(z,\Delta z)|\ |d_j(z,\Delta z)|} = \frac{1}{N_{Vi}}\sum_{j\in V_i} cos\vartheta_{ij}(z,\Delta z) \tag{4}$$

where z is the axial position, Δz is the axial resolution for the displacement calculation, V_i is the Voronoi neighbourhood of the reference fibre i at position z, N_{V_i} is the number of fibres j contained in the neighbourhood, $d_i(z, \Delta z)$ and $d_j(z, \Delta z)$ are the in-plane displacements vectors on the cross-section considered, for the fibre i and its Voronoi neighbours, respectively. Since the displacements approximate the tangent to the fibre path, smoothing of the fibre trajectories was conducted to remove residual noise from the fibre tracking operation [38]. This was done in MATLAB via a *loess* algorithm, which employs a weighted quadratic polynomial. A smoothing factor of 0.15 was used, which corresponds for these datasets to an interpolation span of about 220 μm (about 30 slices). This allows to filter out shorter range effects and highlight longer range collective mobility.

A schematic is shown in Fig. 4. The value of CM varies in [-1,1], where 1 represents perfectly coherent motion where all fibres move parallel and in the same direction, -1 is the case of counter-streaming (fibres moving parallel to each other but in the opposite direction), and the intermediate value 0 represents random motion. This parameter is local and can be mapped on each tape cross-section. In this case, Δz was set to 7.2 μm according to the resolution of the data reduction scheme used. The median value of CM along the z axis is calculated for each fibre to highlight fibre interactions that last through the entire scan volume considered.

3.3. Length of neighbourhood

The fibre contacts within the volume have been analysed by looking at the level of interconnectivity within the tape, with inspiration to the study of bird nests [35] and fibrous scaffolds [45]. The approach follows a similar reasoning as the one used by Fast et al. [26] in analysing variations in fibre composites. The Voronoi neighbourhood of a fibre is in general not constant, but changes due to the movement of the fibres through the volume. A schematic is shown in Fig. 5, where the evolution of a neighbourhood through space is represented by fibres approaching and leaving the vicinity of the reference fibre. The fibre network is analysed here by looking at the axial length for which two fibres remain in close contact before moving to different neighbourhoods. The median distance along the fibre path for which a contact is maintained is defined as length of neighbourhood, or LON:

$$LON(i) = \widetilde{LPN}(i,j)_{j\epsilon V_{ci}} \tag{5}$$

where V_{ci} is the cumulative Voronoi neighbourhood, defined as the multitude of individual fibres that enter the vicinity of fibre i at some point in space, j is a fibre contained in V_{ci}, and $\widetilde{LPN}(i,j)$ represents the median of the pairwise length of neighbourhood LPN between fibre i and each neighbour j. The length of neighbourhood was calculated on the same tessellation generated to determine the collective motion.

4. Results

4.1. Differential tortuosity

Differential tortuosity τ^d was determined as in Equation (2), with its value ranging from about 0.0001 to 0.01 for both tapes, spanning across three orders of magnitude. Assuming that the order of magnitude of the parameter is more representative of differences between fibres compared to its small variations, the logarithm of τ^d was considered for further analysis. The parameter distribution for the two tapes is represented in Fig. 6, highlighting higher differential tortuosity for Tape B compared to Tape A, shown by a shift to higher values. As a reference

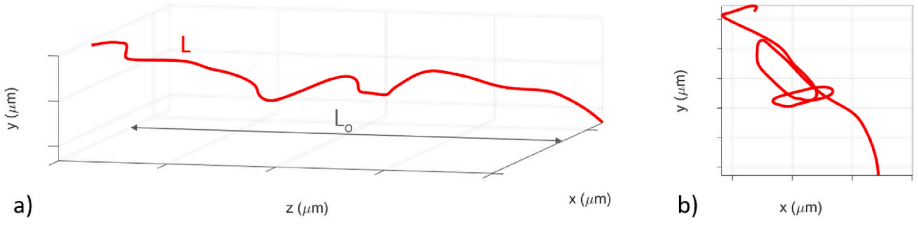

Fig. 3. Example of a tortuous fibre trajectory. The fibre is represented with a solid red line of total length L, in a) 3D, b) 2D view, orthogonal to the tape axis. A volume of length L_0 is shown. (For interpretation of the references to colour in this figure legend, the reader is referred to the Web version of this article.)

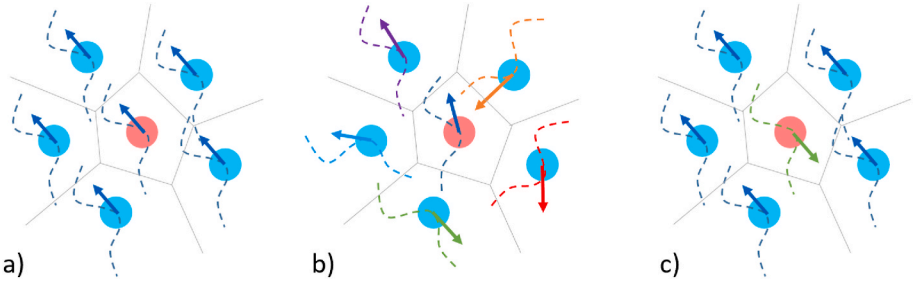

Fig. 4. Application of the collective motion parameter to a particle in its neighbourhood, for a value of a) 1 (synchronous motion) b) 0 (random motion) c) −1 (counter-streaming). The reference fibre centre is highlighted in red, and its immediate neighbours in blue. The local in-plane displacement vector between two slices is shown by an arrow, and the trajectory by a dashed line. (For interpretation of the references to colour in this figure legend, the reader is referred to the Web version of this article.)

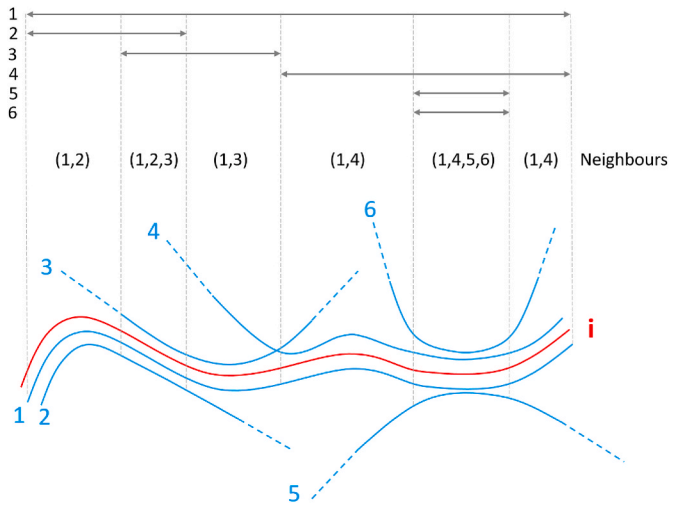

Fig. 5. Concept representing length of neighbourhood (LON) for a 2D case. The neighbourhood of the reference fibre *i* (in red) varies through space, with fibres both approaching and leaving its vicinity. The local neighbourhood is indicated in brackets, while the arrows indicate the pairwise length of neighbourhood LPN between fibre *i* and each neighbour. (For interpretation of the references to colour in this figure legend, the reader is referred to the Web version of this article.)

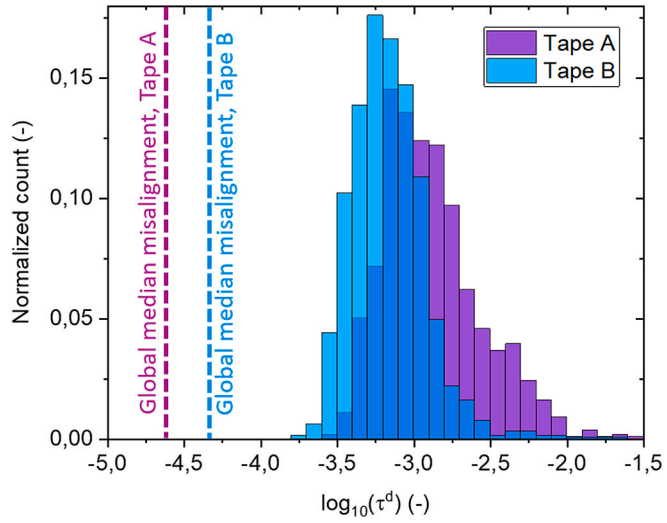

Fig. 6. Histogram of the logarithm of differential tortuosity for the two tapes. The dashed lines represent the tortuosity related to the fibres global median misalignment.

benchmark, the corresponding median value of tortuosity related to the global fibre misalignment is reported as a dashed line. These misalignment values are computed considering only the extreme sections of the scan volume, and therefore perfectly straight fibres: their median values amounts to respectively 0.38° and 0.58° for Tape A and Tape B, corresponding to a logarithm of differential tortuosity of −4.65 and −4.29.

Fig. 7a) and b) represent the projection of all the individual fibre paths on a tape cross-section orthogonal to its axis, colour-coded according to the correspondent value of τ^d.

The parameter varies through the cross-section, with a tendency to higher values towards the tape edges. The differential tortuosity was evaluated in the thickness direction of the tape, corresponding to the *y* axis in Fig. 7a) and b) to characterize this edge effect in greater detail. A bin scatter plot was used to help visualise the distribution of differential tortuosity according to the average *y* position of the fibres. The result is shown in Fig. 7c) and d). The global median of the logarithm of τ^d is shown by a vertical dashed line, while the local median for each horizontal bin is shown by a red square. The error bars represent the upper and lower quartiles. By comparison of the global median to the local median for each *y* value, different regions can be identified. Where the local median at a thickness value is higher than the global median, that region was classified as 'edge', while if lower, as 'core'. Tape A shows, in this case, a more symmetric edge effect of about 30 μm thickness on both sides, while Tape B shows a larger edge effect at the top (about 80 μm) and a smaller edge region towards the bottom edge (15 μm).

4.2. Collective motion

The contour plot of Fig. 8a) and b) represent the median value of collective motion for each fibre, calculated fibre-by-fibre for the full length of (1450 μm). The fibre configuration at the beginning of the measurement volume was used for the representation.

As explained in greater detail in Section 3.2, a value of 1 represents perfectly parallel motion in the same direction, 0 corresponds to random motion, and −1 to counter-streaming. The results show variations through the cross-section, with some regions displaying high levels of coherent motion above a value of $CM = 0.8$, depicted in a lighter colour.

The variation of CM along the tape thickness is shown in Fig. 8c) and d). The global median for the cross-section is shown as a dashed line, while the local median for each thickness level is shown by a red square, together with the interquartile range. Greater collective behaviour is observed at the centre of the tapes compared to the top and bottom edges, which resembles the same edge-core architecture observed for differential tortuosity in Fig. 7c) and d). By comparison of the global and local median, a symmetric edge effect of about 30 μm is observed in Tape A. In Tape B, an edge effect at the top of about 80 μm and of about 10 μm at the bottom is observed.

4.3. Length of neighbourhood

The length of neighbourhood LON was defined as in Equation (5). The parameter corresponds to the median axial distance for which a contact is maintained.

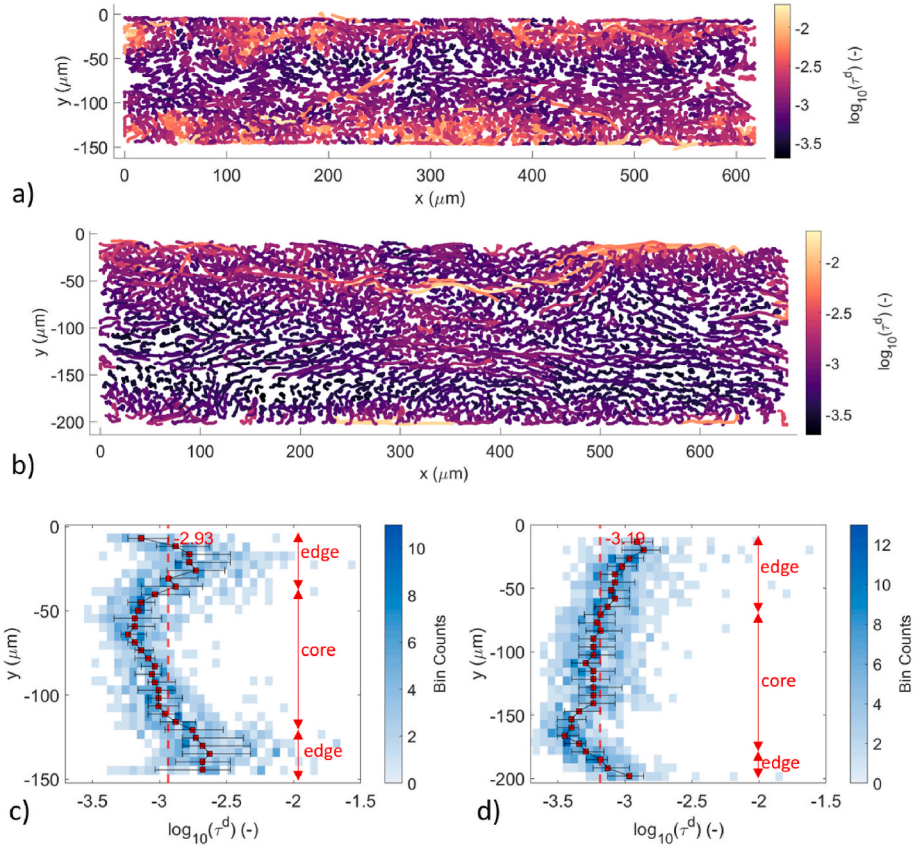

Fig. 7. Projection of the fibre paths on a single cross-section orthogonal to the tape axis, colour - coded according to the logarithm of differential tortuosity (τ^d), for a) Tape A b) Tape B; bin scatter plot of the logarithm of differential tortuosity along the tape thickness for c) Tape A d) Tape B. The dashed line represents the median value of the logarithm of differential tortuosity calculated over the full cross-section, which value is noted at the top of each graph. For each horizontal bin, the local median is represented with red squares. The error bars represent the interquartile range. (For interpretation of the references to colour in this figure legend, the reader is referred to the Web version of this article.)

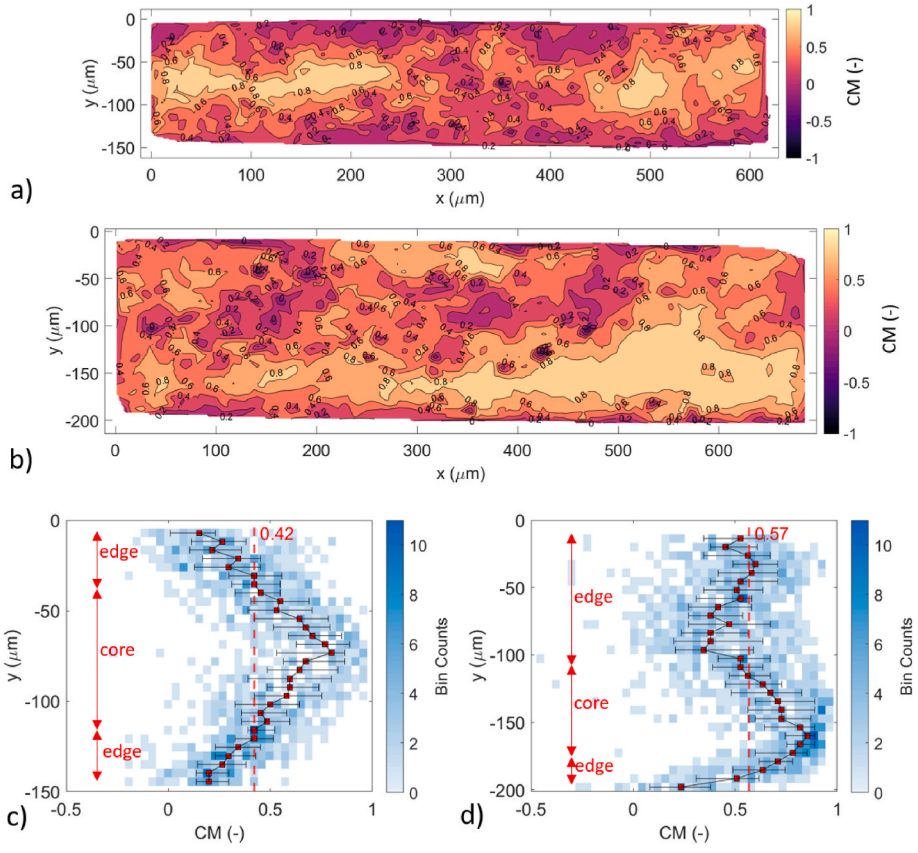

Fig. 8. Contour plot of collective motion (CM) for a) Tape A, b) Tape B; thickness profile for c) Tape A, d) Tape B. The dashed line represents the median calculated over the full cross-section, which value is noted at the top of each graph. For each horizontal bin, the median of the distribution is represented with red squares. The error bars represent the upper and lower quartile. (For interpretation of the references to colour in this figure legend, the reader is referred to the Web version of this article.)

Contour plots for showing the cross-sectional variability of LON can be found for Tape A and Tape B, respectively in Fig. 9a) and b). Bin scatter plots are used to represent the distribution of the parameters in relation to the tape thickness in Fig. 9c) and d). The global median for the cross-section is shown as a dashed line, while the local median for each thickness level is shown by a red square, together with the inter-quartile range. A value of LON of 1450 μm, corresponding to the length of the full observation volume, indicates that a fibre maintains contact with the same neighbours through the entire axial length considered. The results show that LON is not constant through the cross-section, and that a variation through the tape thickness of LON is present. At the upper and lower tape edges, a lower length of neighbourhood is detected, similarly to the edge-core effect previously seen for differential tortuosity and collective motion. In this case, a symmetric edge effect of about 25 μm is observed in Tape A, while in Tape B, the top and bottom edges are respectively of about 90 μm and of about 10 μm.

5. Discussion

The results show that hierarchies in fibre organisation can be found in both samples analysed at all levels of observation. Similarly to the approach used by Song et al. in studying fibre arrangements in natural graded materials by looking at their thickness distribution [34], an edge-core effect can be observed for the three parameters. The approach might be leveraged to gain insight into the mechanisms of microstructural formation of tapes and composites.

5.1. Differential tortuosity

As shown in Fig. 6, the tortuosity distribution is not related to the effect of global fibre misalignment, which is responsible for low tortuosity levels. The differences in tortuosity distribution observed in Fig. 7 by comparing the two tapes might be related to the spreading configuration [46]. If mechanical spreader bars were used, typically both edges of the tape might encounter the spreader bars contact and friction, which is hypothesised to be the cause of the local increase of differential tortuosity τ^d. Impregnation might also play a role in locally affecting the microstructure, with varying effects depending on the impregnation method used [47,48].

The emergence of microstructural variability should be further investigated in relation to the control of the manufacturing parameters and to the tape geometry. By reducing the tape thickness, it is possible that the core region might gradually disappear, and the high tortuosity edge effect would prevail through the entire cross-section. This would be of particular importance in the study of thin ply composites [2].

5.2. Collective motion

Values of collective motion close to 1 suggest the existence of fibre bundles areas with a degree of organisation within the tapes analysed, which was not observed before. Note that in Fig. 8, only a few areas show counter-streaming, indicating it is not prevalent.

The collective motion CM defined here is capable to only capture synchronised displacement. It is however possible that high tortuosity fibres might undergo other types of collective motion patterns which could be related, for example, to local bundle rotation, which is here not quantified. Further studies should extend the current methodology for a greater understanding of the tape spatial organisation.

5.3. Length of neighbourhood

In a network composed of perfectly straight and parallel fibres, the length of neighbourhood LON should always be equal to the length of the scan volume since their neighbours will not change through space. Conversely, as shown in Fig. 9, the global median of LON has a value of respectively 662 μm and 731 μm for Tape A and Tape B, which

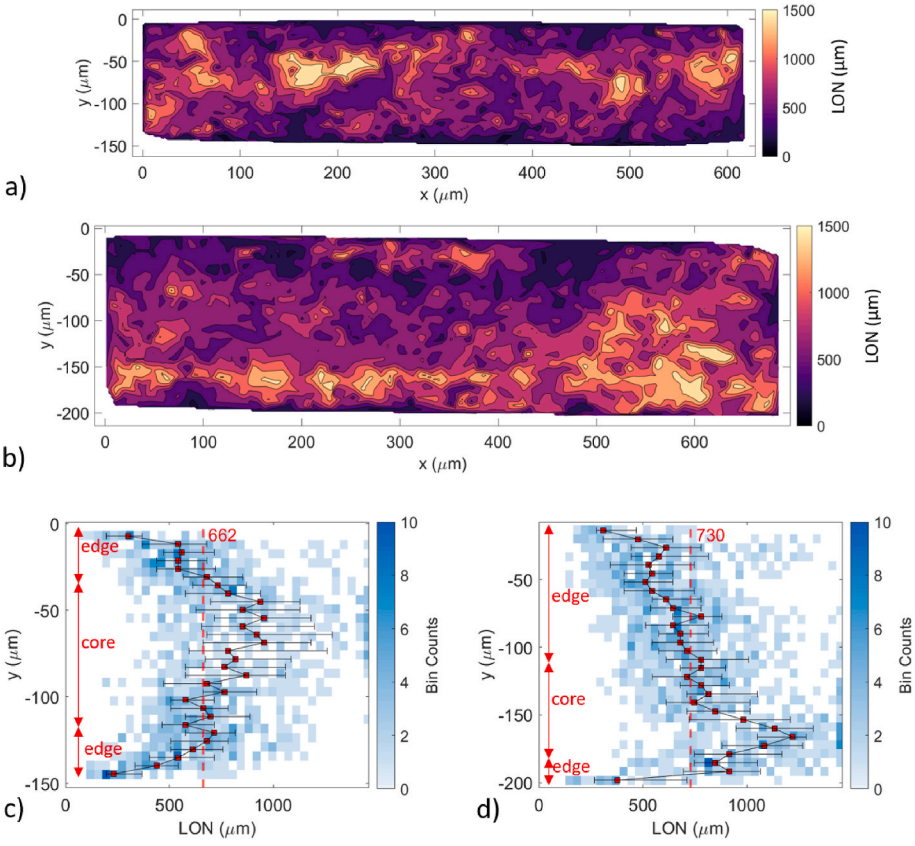

Fig. 9. Contour plot of length of neighbourhood (LON) for a) Tape A, b) Tape B; thickness profile for c) Tape A, d) Tape B. The dashed line represents the median calculated over the full cross-section, which value is noted at the top of each graph. For each horizontal bin, the median of the distribution is represented with red squares. The error bars represent the interquartile range. (For interpretation of the references to colour in this figure legend, the reader is referred to the Web version of this article.)

corresponds to about half of the length of observation L_o. This means that two fibres will generally remain in close contact for about 700 μm before moving to different neighbourhoods.

In both tapes, fibres that have not yet changed neighbourhood can be identified in the bin scatter by points located at LON = L_o, in this case equal to 1450 μm. Such fibres have been defined as 'invariant fibres' in the work of Fast et al., since their neighbourhood does not vary [26]. This is however a feature related to the size of the scan volume. Such fibres might change neighbours later on along the tape, and a larger length of observation is required to confirm this.

This concept was further explored by artificially varying the length of the scan volume L_o, from a value of 0 to the value of the total length of observation of 1450 μm. Fig. 10 shows the variation in the percentage of fibres having LON $< L_o$ which therefore have exchanged neighbours at least once in the volume, as a function of L_o. For a very small value of L_o, the microstructure resembles an ideal unidirectional composite, with most fibres remaining in the same neighbourhood through the entire length of observation. An increasingly long scan volume is able to start capturing the deviations from the ideal model, capturing the variability in LON within the material.

Eventually, all fibres are expected to have exchanged neighbours at least once. According to Fig. 10, this seems to occur earlier in Tape A compared to Tape B, which can be observed by a shift of the curve towards lower L_o values. This aligns with the ordering of the global median values shown in Fig. 9 and might reflect a greater extent of neighbourhood variation related to its overall greater differential tortuosity. For the maximum scan volume observed of 1450 μm, both tapes reach a value of about 97% of fibres which satisfy the condition of LON $< L_o$, indicating that such scan length is sufficient for the given materials to extract the full LON distribution. We therefore expect that a further increase of the scan volume would not significantly change the trends shown for this parameter.

Such scan volume size might represent a characteristic length of fibre association, describing the level of interconnectivity within the material. By capturing the periodicity of the fibre association, this approach might guide future work in defining the axial dimension of representative volume elements (RVE) for more accurate modelling of unidirectional composites [49,50].

5.4. Interrelation of parameters

By further studying the parameter interrelation, more information can be gathered on the architecture of the material. Due to the similar edge-core effect and edge-core thickness observed for both differential tortuosity and collective motion, the relationship between the two parameters was further investigated.

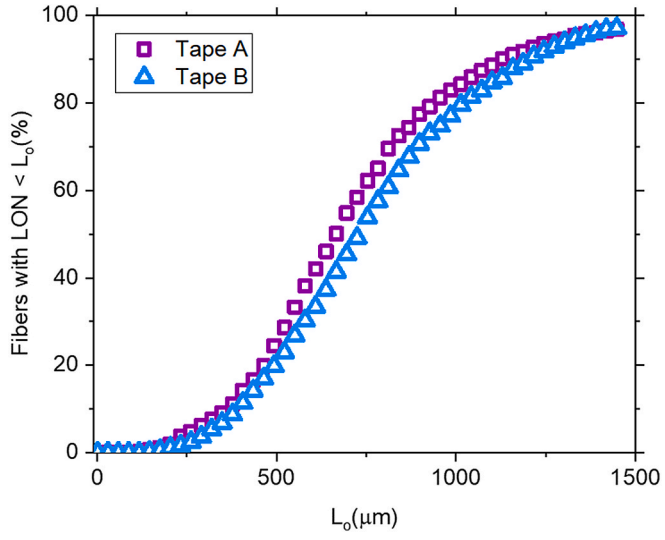

Fig. 10. Fraction of fibres with a length of neighbourhood LON lower than the volume scan size L_o, for varying L_o.

Fig. 11a) and b) show a bin scatter plot comparing τ^d and CM. For the two tape portions analysed, there is a tendency for regions of lower differential tortuosity to move with greater coherence. Conversely, fibres that show high differential tortuosity show a lower tendency to coherent motion, which might translate into the presence of lone fibres moving independently from their surroundings, as the 'stray fibres' observed in literature at the free surface of UDCs [24]. Such an approach has the potential to identify different regimes in the fibre organisation in a material, which should be related to the manufacturing or processing methods.

LON was analysed in relation to the logarithm of τ^d and CM, as shown in Fig. 12. In both tapes, fibres that have a lower length of neighbourhood tend to move less collectively and have higher differential tortuosity. Conversely, a higher LON is associated with a higher tendency to collective behaviour and lower differential tortuosity. This agrees with the observation that at lower differential tortuosity, fibres might tend to have greater alignment and remain close to their original neighbourhood. It also seems to indicate that a more coherent fibre association and movement through the volume might be associated with a higher length of neighbourhood and lower tortuosity.

The quantification of these descriptors might find application both in tape manufacturing, and in the study of microstuctural evolution during composite part formation. Microstructural variability can affect deconsolidation [15], consolidation [51] or microstructural conditioning [4]. Ultimately, the proposed methods might contribute towards the development of tailored microstructures for specific applications.

6. Conclusion

Understanding the three-dimensional variability of unidirectional composites is relevant for the development of advanced material modelling strategies. In this work, a novel methodology was developed for the characterization of continuous unidirectional composites. 3D microstructural descriptors were introduced, covering trajectory analysis (differential tortuosity), group behaviour (collective motion), and network connectivity (length of neighbourhood), each representing an increasing level of complexity in the fibre architecture. These key descriptors were showcased on real material datasets from two different CF/PEEK tapes. 3D scan volumes were acquired via X-ray computed tomography, and a facile method for image analysis was used to reconstruct the 3D fibrous architecture at a single fibre path resolution.

Single fibre trajectories are described by a novel definition called differential tortuosity, which highlights the deviation of the fibre trajectory from a straight longitudinal path. The group behaviour analysis is conducted by the collective motion concept, inspired by animal locomotion, that can detect synchronous fibre bundle motion. The fibre network connectivity was evaluated by a length of neighbour contact definition that relies on the axial distance in which fibres remain in the same Voronoi neighbourhood. It was shown that these proposed descriptors enable to highlight micro- and mesoscopic features. Key observations based on these material sets are as follows. Similar through-thickness gradients, in the form of edge-core effects, were observed for all three parameters. The study of parameter interdependence was able to further describe the architectural arrangement at a single fibre resolution. For both tapes analysed, fibres with higher differential tortuosity, therefore greater deviations from the ideal longitudinal direction, show both a lower tendency to move collectively and a lower length of neighbourhood, indicating a more independent movement from their neighbourhood. Conversely, a higher length of neighbourhood is associated with a higher tendency to collective behaviour and lower differential tortuosity.

Another interesting observation is related to the effect of scanned tape length on the evolution of the length of neighbourhood (LON). The

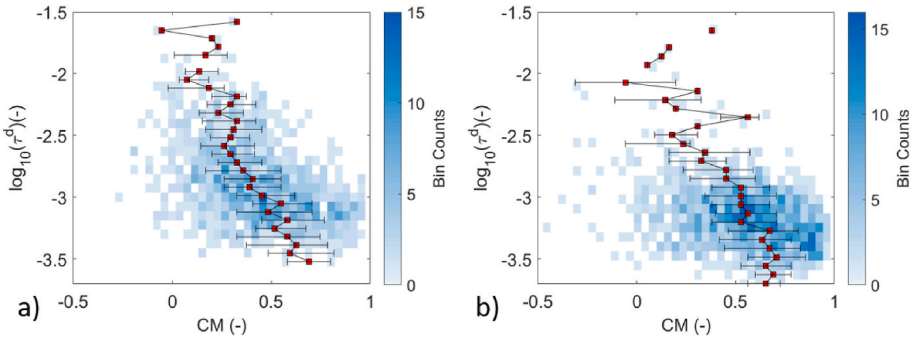

Fig. 11. Collective motion CM against logarithm of differential tortuosity τ^d for a) Tape A, and b) Tape B. For each horizontal bin, the median of the distribution is represented with red squares. The error bars represent the quartile interval. (For interpretation of the references to colour in this figure legend, the reader is referred to the Web version of this article.)

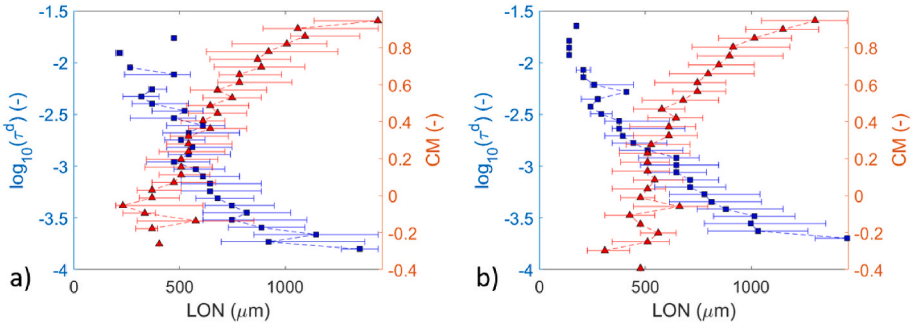

Fig. 12. Length of neighbourhood as a function of differential tortuosity and collective motion for a) Tape A, and b) Tape B. The blue squares correspond to the median logarithm of differential tortuosity (left axis), while the red triangles correspond to the median collective motion (right axis). The error bars represent the interquartile range. (For interpretation of the references to colour in this figure legend, the reader is referred to the Web version of this article.)

maximum value of LON is bound to the size of the scanned volume. By increasing the axial size of the scan volume, the change of fibre contacts can be increasingly sampled. Given a long enough volume, all fibres will have changed neighbours at least once. For the tapes analysed, the axial size for which this happens was found to be 1450 μm. Such volume size constitutes a characteristic length for a unidirectional material and relates to its level of fibre interconnectivity. This provides both insight on the network arrangement and a guideline for future work in the definition of representative scan volumes.

The work contributes to bridging a gap in the classical approach and nomenclature typical of the composite field to describe and quantify complex architectural organization, by successfully employing strategies inspired by other research domains. The novel parameters introduced enable new routes for the description and quantification of complex fibre arrangements. This methodology for the analysis of UDCs might allow distinguishing different regimes of fibre organisation in similar fibre-resin systems and might also be applicable in general to the description of the architecture of fibrous material.

The parameters shown here and their interdependence will provide further insight into micro- and mesoscopic effects related to microstructure formation of UDCs. Future work will study the influence on the microstructure of the choice of manufacturing parameters, such as fibre spreading and impregnation, and the propagation of the architectural features at various lengthscales. Microstructural evolution during processing or loading could also be studied with this approach. The understanding of the scale of organisation in a material, as through the length of neighbourhood, might provide input for advanced modelling techniques such as RVE.

Author contributions

Silvia Gomarasca: Conceptualization, Methodology, Validation, Formal Analysis, Investigation, Writing - Original Draft; **Daniël Peeters**: Conceptualization, Supervision, Writing - Review and Editing; **Bilim Atli-Veltin**: Supervision, Writing - Review and Editing; **Clemens Dransfeld**: Conceptualization, Methodology, Supervision, Writing - Review and Editing, Project Administration.

Funding sources

This research did not receive any specific grant from funding agencies in the public, commercial, or not-for-profit sectors.

Declaration of competing interest

The authors declare that they have no known competing financial interests or personal relationships that could have appeared to influence the work reported in this paper.

Acknowledgements

The authors would like to acknowledge Naturalis Biodiversity Center, Leiden (NL) for conducting the data acquisition via X-ray computed tomography.

References

[1] F. Malgioglio, S. Pimenta, A. Matveeva, L. Farkas, W. Desmet, S.V. Lomov, Y. Swolfs, Microscale material variability and its effect on longitudinal tensile failure of unidirectional carbon fibre composites, Compos. Struct. 261 (2020) 113300.

[2] R. Amacher, J. Cugnoni, J. Botsis, L. Sorensen, W. Smith, C. Dransfeld, Thin ply composites: experimental characterization and modeling of size-effects, Compos. Sci. Technol. 101 (2014) 121–132.

[3] P. Parandoush, D. Lin, A review on additive manufacturing of polymer-fiber composites, Compos. Struct. 182 (2017) 36–53.

[4] M. Eichenhofer, J.C. Wong, P. Ermanni, Exploiting cyclic softening in continuous lattice fabrication for the additive manufacturing of high performance fibre-reinforced thermoplastic composite materials, Compos. Sci. Technol. 164 (May, 2018) 248–259.
[5] T.H. Vaneker, Material extrusion of continuous fiber reinforced plastics using commingled yarn, Procedia CIRP 66 (2017) 317–322.
[6] A. Thakur, X. Dong, Printing with 3D continuous carbon fiber multifunctional composites via UV-assisted coextrusion deposition, Manufact. Lett. 24 (2020) 1–5.
[7] B.R. Denos, D.E. Sommer, A.J. Favaloro, R.B. Pipes, W.B. Avery, Fiber orientation measurement from mesoscale CT scans of prepreg platelet molded composites, Compos. Appl. Sci. Manuf. 114 (August, 2018) 241–249.
[8] N.Q. Nguyen, M. Mehdikhani, I. Straumit, L. Gorbatikh, L. Lessard, S.V. Lomov, Micro-CT measurement of fibre misalignment: application to carbon/epoxy laminates manufactured in autoclave and by vacuum assisted resin transfer moulding, Compos. Appl. Sci. Manuf. 104 (2018) 14–23.
[9] T. Baranowski, D. Dobrovolskij, K. Dremel, A. Hölzing, G. Lohfink, K. Schladitz, S. Zabler, Local fiber orientation from X-ray region-of-interest computed tomography of large fiber reinforced composite components, Compos. Sci. Technol. 183 (February, 2019) 107786.
[10] T.A. Sebaey, G. Catalanotti, N.P. O'Dowd, A microscale integrated approach to measure and model fibre misalignment in fibre-reinforced composites, Compos. Sci. Technol. 183 (June, 2019) 107793.
[11] R. Belliveau, É. Léger, B. Landry, G. LaPlante, Measuring fibre orientation and predicting elastic properties of discontinuous long fibre thermoplastic composites, J. Compos. Mater. 55 (3) (2020) 321–330.
[12] L. Schöttl, D. Dörr, P. Pinter, K.A. Weidenmann, P. Elsner, L. Kärger, A novel approach for segmenting and mapping of local fiber orientation of continuous fiber-reinforced composite laminates based on volumetric images, NDT E Int. 110 (June 2019) 2020.
[13] F. Gommer, A. Endruweit, A.C. Long, Analysis of filament arrangements and generation of statistically equivalent composite micro-structures, Compos. Sci. Technol. 99 (2014) 45–51.
[14] M. Mehdikhani, C. Breite, Y. Swolfs, M. Wevers, S.V. Lomov, L. Gorbatikh, Combining digital image correlation with X-ray computed tomography for characterization of fiber orientation in unidirectional composites, Compos. Appl. Sci. Manuf. 142 (2021) 106234.
[15] T.K. Slange, L.L. Warnet, W.J. Grouve, R. Akkerman, Deconsolidation of C/PEEK blanks: on the role of prepreg, blank manufacturing method and conditioning, Compos. Appl. Sci. Manuf. 113 (July, 2018) 189–199.
[16] G. Catalanotti, T. Sebaey, An algorithm for the generation of three-dimensional statistically Representative Volume Elements of unidirectional fibre-reinforced plastics: focusing on the fibres waviness, Compos. Struct. 227 (2019) 111272.
[17] F. Gommer, K.C.A. Wedgwood, L.P. Brown, Composites : Part A Stochastic reconstruction of filament paths in fibre bundles based on two-dimensional input data, Composites Part A: Applied Science and 555 Manufacturing 76 (2015) 262–271.
[18] M.J. Emerson, K.M. Jespersen, A.B. Dahl, K. Conradsen, L.P. Mikkelsen, Individual fibre segmentation from 3D X-ray computed tomography for characterising the fibre orientation in unidirectional composite materials, Compos. Appl. Sci. Manuf. 97 (2017) 83–92.
[19] M.J. Emerson, V.A. Dahl, K. Conradsen, L.P. Mikkelsen, A.B. Dahl, Statistical validation of individual fibre segmentation from tomograms and microscopy, Compos. Sci. Technol. 160 (January, 2018) 208–215.
[20] K. Amjad, W.J. Christian, K. Dvurecenska, M.G. Chapman, M.D. Uchic, C. P. Przybyla, E.A. Patterson, Computationally efficient method of tracking fibres in composite materials using digital image correlation, Compos. Appl. Sci. Manuf. 129 (2020) 105683.
[21] J. Jhawar, R.G. Morris, U.R. Amith-Kumar, M. Danny Raj, T. Rogers, H. Rajendran, V. Guttal, Noise-induced schooling of fish, Nat. Phys. 16 (No. 4) (2020) 488–493.
[22] R. Karamov, L.M. Martulli, M. Kerschbaum, I. Sergeichev, Y. Swolfs, S.V. Lomov, Micro-CT based structure tensor analysis of fibre orientation in random fibre composites versus high-fidelity fibre identification methods, Compos. Struct. 235 (2020) 111818.
[23] A.T. Zehnder, V. Patel, T.J. Rose, Micro-CT imaging of fibers in composite laminates under high strain bending, Exp. Tech. 44 (5) (2020) 531–540.
[24] N.K. Fritz, R. Kopp, A.K. Nason, X. Ni, J. Lee, I.Y. Stein, E. Kalfon-Cohen, I. Sinclair, S.M. Spearing, P.P. Camanho, B.L. Wardle, New interlaminar features and void distributions in advanced aerospace-grade composites revealed via automated algorithms using micro-computed tomography, Compos. Sci. Technol. 193 (2020) 108132.
[25] Y. Wang, M.J. Emerson, K. Conradsen, A.B. Dahl, V.A. Dahl, E. Maire, P.J. Withers, Evolution of fibre deflection leading to kink-band formation in unidirectional glass fibre/epoxy composite under axial compression, Compos. Sci. Technol. (2021) 108929.
[26] T. Fast, A.E. Scott, H.A. Bale, B.N. Cox, Topological and Euclidean metrics reveal spatially nonuniform structure in the entanglement of stochastic fiber bundles, J. Mater. Sci. 50 (6) (2015) 2370–2398.
[27] F. LeBel, A.E. Fanaei, É. Ruiz, F. Trochu, Experimental characterization by fluorescence of capillary flows in the fiber tows of engineering fabrics, Open J. Inorg. Non-Metallic Mater. 02 (03) (2012) 25–45.
[28] W. Szmyt, C. Guerra-Nuñez, C. Dransfeld, I. Utke, Solving the inverse Knudsen problem: gas diffusion in random fibrous media, J. Membr. Sci. 620 (August 2020) 2021.
[29] N.-j. Jan, B.L. Brazile, D. Hu, G. Grube, J. Wallace, A. Gogola, I.A. Sigal, Crimp around the globe ; patterns of collagen crimp across the corneoscleral shell, Exp. Eye Res. 172 (April, 2018) 159–170.
[30] T. Vicsek, A. Zafeiris, Collective motion, Phys. Rep. 517 (3–4) (2010) 71–140.
[31] E. Méhes, T. Vicsek, Collective motion of cells: from experiments to models, Integr. Biol. 6 (9) (2014) 831–854.
[32] G.K. Taylor, M.S. Triantafyllou, C. Tropea, Animal Locomotion, Springer, 2010.
[33] M. Nagy, Z. Ákos, D. Biro, T. Vicsek, Hierarchical group dynamics in pigeon flocks, Nature 464 (7290) (2010) 890–893.
[34] W. Song, C. Zhang, Z. Wang, Investigation of the microstructural characteristics and the tensile strength of silkworm cocoons using X-ray micro computed tomography, Mater. Des. 199 (2021) 109436.
[35] H.R. Jessel, L. Aharoni, S. Efroni, I. Bachelet, A modeling algorithm for exploring the architecture and construction of bird nests, Sci. Rep. 9 (1) (2019) 1–9.
[36] S. Gantenbein, K. Masania, W. Woigk, J.P. Sesseg, T.A. Tervoort, A.R. Studart, Three-dimensional printing of hierarchical liquid-crystal-polymer structures, Nature 561 (7722) (2018) 226–230.
[37] J. Viguié, P. Latil, L. Orgéas, P.J. Dumont, S. Rolland du Roscoat, J.F. Bloch, C. Marulier, O. Guiraud, Finding fibres and their contacts within 3D images of disordered fibrous media, Compos. Sci. Technol. 89 (2013) 202–210.
[38] P.J. Creveling, W.W. Whitacre, M.W. Czabaj, A fiber-segmentation algorithm for composites imaged using X-ray microtomography : development and validation, Composites Part A 126 (August, 2019) 105606.
[39] J. Schindelin, I. Arganda-Carreras, E. Frise, V. Kaynig, M. Longair, T. Pietzsch, S. Preibisch, C. Rueden, S. Saalfeld, B. Schmid, J.Y. Tinevez, D.J. White, V. Hartenstein, K. Eliceiri, P. Tomancak, A. Cardona, Fiji: an open-source platform for biological-image analysis, Nat. Methods 9 (7) (2012) 676–682.
[40] D.G. Lowe, Distinctive image features from scale-invariant keypoints, Int. J. Comput. Vis. 60 (2) (2004) 91–110.
[41] I. Arganda-Carreras, V. Kaynig, C. Rueden, K.W. Eliceiri, J. Schindelin, A. Cardona, H.S. Seung, Trainable Weka Segmentation: a machine learning tool for microscopy pixel classification, Bioinformatics 33 (15) (2017) 2424–2426.
[42] J.Y. Tinevez, N. Perry, J. Schindelin, G.M. Hoopes, G.D. Reynolds, E. Laplantine, S. Y. Bednarek, S.L. Shorte, K.W. Eliceiri, TrackMate: an open and extensible platform for single-particle tracking, Methods 115 (2017) 80–90.
[43] N. Chenouard, I. Smal, F. De Chaumont, M. Maška, I.F. Sbalzarini, Y. Gong, J. Cardinale, C. Carthel, S. Coraluppi, M. Winter, A.R. Cohen, W.J. Godinez, K. Rohr, Y. Kalaidzidis, L. Liang, J. Duncan, H. Shen, Y. Xu, K.E. Magnusson, J. Jaldén, H.M. Blau, P. Paul-Gilloteaux, P. Roudot, C. Kervrann, F. Waharte, J. Y. Tinevez, S.L. Shorte, J. Willemse, K. Celler, G.P. Van Wezel, H.W. Dan, Y.S. Tsai, C.O. De Solórzano, J.C. Olivo-Marin, E. Meijering, Objective comparison of particle tracking methods, Nat. Methods 11 (3) (2014) 281–289.
[44] R.J. Mandle, J. Goodby, Order parameters, orientational distribution functions and heliconical tilt angles of oligomeric liquid crystals, Phys. Chem. 21 (13) (2019) 6839–6843.
[45] J. Maksimcuka, A. Obata, W.W. Sampson, R. Blanc, C. Gao, P.J. Withers, O. Tsigkou, T. Kasuga, P.D. Lee, G. Poologasundarampillai, X-ray tomographic imaging of tensile deformation modes of electrospun biodegradable polyester fibers, Front. Mater. 4 (December, 2017) 1–11.
[46] M.S. Irfan, V.R. MacHavaram, R.S. Mahendran, N. Shotton-Gale, C.F. Wait, M. A. Paget, M. Hudson, G.F. Fernando, Lateral spreading of a fiber bundle via mechanical means, J. Compos. Mater. 46 (3) (2012) 311–330.
[47] J. Studer, C. Dransfeld, J. Jauregui Cano, A. Keller, M. Wink, K. Masania, B. Fiedler, Effect of fabric architecture, compaction and permeability on through thickness thermoplastic melt impregnation, Compos. Appl. Sci. Manuf. 122 (April, 2019) 45–53.
[48] K.K. Ho, S.R. Shamsuddin, S. Riaz, S. Lamorinere, M.Q. Tran, A. Javaid, A. Bismarck, Wet impregnation as route to unidirectional carbon fibre reinforced thermoplastic composites manufacturing, Plastics, Rubber Compos. 40 (2) (2011) 100–107.
[49] W. Wang, Y. Dai, C. Zhang, X. Gao, M. Zhao, Micromechanical modeling of fiber-reinforced composites with statistically equivalent random fiber distribution, Materials 9 (8) (2016) 1–14.
[50] L. Varandas, G. Catalanotti, A. Melro, R. Tavares, B. Falzon, Micromechanical modelling of the longitudinal compressive and tensile failure of unidirectional composites: the effect of fibre misalignment introduced via a stochastic process, Int. J. Solid Struct. 203 (2020) 157–176.
[51] O. Çelik, D. Peeters, C. Dransfeld, J. Teuwen, Intimate contact development during laser assisted fiber placement: microstructure and effect of process parameters, Compos. Appl. Sci. Manuf. 134 (2020) 105888.